

Parametric Sensitivity Analysis for Stochastic Molecular Systems using Information Theoretic Metrics

Anastasios Tsourtis,^{1, a)} Yannis Pantazis,^{2, b)} Markos A. Katsoulakis,^{2, c)} and Vagelis Harmandaris^{3, d)}

¹⁾*Department of Mathematics and Applied Mathematics, University of Crete, Greece*

²⁾*Department of Mathematics and Statistics, University of Massachusetts, Amherst, USA*

³⁾*Department of Mathematics and Applied Mathematics, University of Crete, Institute of Applied and Computational Mathematics (IACM), Foundation for Research and Technology Hellas (FORTH), GR-70013, Heraklion, Crete, Greece*

(Dated: November 5, 2018)

In this paper we extend the parametric sensitivity analysis (SA) methodology proposed in Ref. [Y. Pantazis and M. A. Katsoulakis, J. Chem. Phys. 138, 054115 (2013)]

to continuous time and continuous space Markov processes represented by stochastic differential equations and, particularly, stochastic molecular dynamics as described by the Langevin equation. The utilized SA method is based on the computation of the information-theoretic (and thermodynamic) quantity of relative entropy rate (RER) and the associated Fisher information matrix (FIM) between path distributions. A major advantage of the pathwise SA method is that both RER and pathwise FIM depend only on averages of the force field therefore they are tractable and computable as ergodic averages from a single run of the molecular dynamics simulation both in equilibrium and in non-equilibrium steady state regimes. We validate the performance of the extended SA method to two different molecular stochastic systems, a standard Lennard-Jones fluid and an all-atom methane liquid and compare the obtained parameter sensitivities with parameter sensitivities on three popular and well-studied observable functions, namely, the radial distribution function, the mean squared displacement and the pressure. Results show that the RER-based sensitivities are highly correlated with the observable-based sensitivities.

Keywords: Relative Entropy, Sensitivity Analysis, Fisher Information Matrix, Langevin dynamics, Methane Molecular Dynamics

I. INTRODUCTION

Molecular simulation is the bridge between theoretically developed models and experimental approaches for the study of molecular systems in the atomistic level.¹ Nowadays, molecular simulation methodologies are used extensively to predict structure-properties relations of complex systems. The importance of numerical simulations in material sciences, biology and chemistry has been recently acknowledged by the 2013 Nobel price in Chemistry “for the development of multiscale models in complex chemical systems”. The computational modeling of realistic complex molecular systems at the molecular level requires long molecular simulations for an enormous distribution of length and time scales.^{2–5} The properties of the model systems depend on a large number of parameters, which are usually obtained utilizing optimization techniques matching specific data taken either from more detailed (e.g. ab-initio) simulations or from experiments. Furthermore, stochastic modeling is especially important

for describing the inherent randomness of molecular dynamics in various scales.

All the above complexities imply the need of rigorous mathematical tools for the analysis of both deterministic and stochastic molecular systems. Uncertainty quantification (UQ) in computational chemistry is of paramount importance, especially in multiscale modeling, where properties evaluated at the atomic-molecular scale are transferred to the mesoscopic scale.^{4,6} Sources of epistemic uncertainty can stem from (i) numerical uncertainty, (ii) model uncertainty and (iii) parametric uncertainty. Numerical uncertainties are related to the finite time of the dynamic simulation, the number of particles, as well as values of the parameters related to the numerical method used (e.g. time-step), to name some. Model uncertainty comes from the specific force field representation and its calibration to experimental properties, and the usage of specific boundary conditions. Parametric uncertainties stem from errors in parameter values due to noisy or insufficient measurements. Of all the above, the uncertainty associated with the parameters of the potential is the least understood.^{6,7} Furthermore, intrinsic stochasticity of the system is added on top of epistemic uncertainty. This type of uncertainty is also called aleatoric.

There exists a diverse range of UQ approaches pro-

^{a)}E-mail: tsourtis@uoc.gr

^{b)}E-mail: yannis.pantazis@gmail.com

^{c)}E-mail: markos@math.umass.edu

^{d)}E-mail: harman@uoc.gr

posed in the literature. Variance-based methods such as analysis of variance (ANOVA),⁸ Bayesian statistical analysis^{7,9} (applications to deal with large uncertainties) and polynomial chaos expansions¹⁰ have been widely used. The first two methods are based on multiple and usually expensive Monte Carlo runs resulting in huge computational cost whereas the latter becomes intractable when the parameter space is large. An in depth study of this last method in MD has recently been presented by Rizzi et al.¹⁰

Sensitivity analysis (SA) is a powerful tool that gives insight of how small variations (uncertainty) in system parameters (input), can affect the output of the system substantially. Such perturbations occur from computational errors, uncertainty and errors resulting from experimental parameter estimation¹¹ (such as parameter fitting through ensemble averages of macroscopic thermodynamic quantities). Thus, parametric SA can provide critical insights in uncertainty quantification. Especially in the stochastic setting (e.g., Langevin dynamics in molecular systems), SA is performed by analysis of the system’s mean behavior, i.e., several simulations starting from a configuration at the stationary (or steady states) regime. The stationary regime is crucial for complex molecular systems since it captures not only static quantities such as the radial distribution function but also dynamical quantities which includes transitions between metastable states in complex, high-dimensional energy landscapes and intermittency.¹² Depending on the magnitude of the perturbations, SA can be classified into local (infinitesimal, one-at-a-time parameter perturbation) and global (finite, multiple parameter perturbation).

Furthermore, the role of SA is not restricted to UQ but it is of pivotal significance in several other applications. First, robustness of a system meaning the stability of the behavior under simultaneous changes in model parameters or variations of orders of magnitude in insensitive parameters that insignificantly affect the dynamics can be addressed utilizing parametric SA approaches. Second, sensitivity analysis on experiment conditions under which information loss is minimized, establish optimal experimental design.¹³ Furthermore, identifiability analysis employs SA to determine a priori whether certain parameters can be estimated from experimental data of a given type. The work in Ref. 14 contains a general framework of SA in MD (proteins) using the observable helicity while cross-validation with experimental data is also displayed. Overall, SA plays a fundamental role in multiscale design and as it has been highlighted by Braatz et al.¹⁵.

Typically in a stochastic setting, the most common local parametric SA method is based on partial derivatives on ensemble averages of quantities of interest around a nominal parameter value.¹⁶ Large derivatives indicate strong sensitivity of the observable to the particular parameter while the opposite holds when the derivative values are small. There has been an increasing number of methods to compute the partial derivatives especially

in discrete-event systems whose applications range from biochemical reaction networks to operations research and queuing theory. Finite-difference approaches based on common random numbers,¹⁶ on common reaction path¹⁷ which exploits positive correlations among coupled perturbed/unperturbed reaction paths as well as coupling methods^{18,19} have been proposed. There are certain issues associated with these finite-difference approaches; the estimator of the partial derivative has bias while the variance of the gradient estimator increases with the dimension of the parameter space. Instead of using the finite-difference approaches, one can utilize Girsanov measure transformation to directly compute the infinitesimal sensitivity.^{20–22} In MD simulations where both time and states are typically continuous, Iordanov et al.²³ performed SA in three potentials of different functional forms (and number of parameters) in order to compare their influence in thermodynamic quantities. Instead of perturbing the potential parameters they scaled the potentials one-at-a-time (local SA) aiming to minimize the discrepancy from the experimental values of each observable separately.

Another class of sensitivity methods which is not focused on specific observable functions but on the overall properties of the stochastic process is based on information theory concepts. Application of information-theoretic SA methods to analysis of stochastic models uses quantities such as entropy, relative entropy (or Kullback-Leibler divergence), the corresponding Fisher information matrix as well as mutual information. Relative entropy (RE) measures the inefficiency of assuming a perturbed (or "wrong") distribution instead of assuming the unperturbed (or "true") one. RE have been used for the SA study of climate models²⁴ where the equilibrium probability density function (PDF) has been obtained through an entropy maximization subject to constraints induced by the measurements, while Fisher information matrix (FIM) is an indispensable tool for optimal experimental design.¹³ In a typical SA approach based on RE, explicit knowledge of the equilibrium PDF is assumed. However, in systems with non-equilibrium steady states (NESS) (i.e., systems in which a steady state is reached but the detailed balance condition is violated), there are no explicit formulas for the stationary distribution and even when a Gibbs measure is available, it is usually computationally inefficient to sample from. Such non-equilibrium systems are common place in molecular systems with multiple mechanisms such as reaction-diffusion systems or driven molecular systems.²⁵

In Ref. 12, the RE between path distributions (i.e., distributions of the particle trajectories) for discrete time or discrete event systems was been utilized as a measure of sensitivity. When the system is in stationarity the relative entropy of the two path distributions decomposes into two parts; (i) the relative entropy rate (RER) that scales linearly with time and (ii) a constant term related to the relative entropy of the initial distribution of the system. In long times, the first term dominates

providing major insights on the sensitivity of the system with respect to parameter perturbations. In this work, we extend the SA method proposed in Ref. 12 to the case of stochastic differential equations (i.e., continuous-time and continuous state space) and particularly the Langevin equation. Furthermore, when perturbations are small, a Taylor expansion on RER is performed revealing the lower order of this expansion which is the pathwise FIM associated with the RER. Practically, RER is an observable of the stochastic process which can be computed numerically as an ergodic average in a straightforward manner as it only requires local dynamics (in our case the forces). Similarly, FIM computations are feasible in the same fashion with the advantage of being more informative since any perturbation direction can be explored. Both of these observables can be sampled on the fly, from a single MD run since only the reference process needs to be simulated. Finally, spectral methods for the calculation of RER were introduced for the over-damped Langevin case in Ref. 26.

The studied pathwise SA method has major advantages which can be listed as follows. First, it is gradient-free method which does not require knowledge of the equilibrium PDF. By gradient-free we mean that the pathwise FIM does not depend on the extent of the perturbation, so when the computation for different perturbations is necessary (especially in high-dimensional problems) the extra cost is minimal in comparison to the straightforward RER calculation. Second, it is rigorously valid for long-time, stationary dynamics in path-space including metastable dynamics in a complex landscape. Third, it is suitable for non-equilibrium systems from statistical mechanics perspective; for example in NESS processes such as dissipative systems where the structure of the equilibrium PDF is unknown. Fourth, it is fast since it requires samples only from the unperturbed process which can be also obtained in a trivially parallel manner.

The work presented here is a part of a more general hierarchical simulation scheme that involves multiple simulation level and a broad range of length and time scales.²⁷⁻²⁹ In this work, we apply the above methodology on stochastic molecular systems as the RER and FIM methods are based on this setting i.e., non-deterministic with random noise. As test cases we examine: (a) a benchmark Lennard-Jones (LJ) fluid model,^{1,30} and, (b) a detailed all-atom methane (CH_4) model.³¹ The LJ fluid system is the most widely used in molecular simulations model of a simple fluid, whereas the second one employs more complexity due to the intramolecular bond and angle potentials in addition to the LJ intermolecular potential. Methane has been also extensively studied over the years due to the fact that it is in abundance in nature and has environmental impacts as well as it can be used as fuel being the main component of natural gas.

The proposed pathwise SA method is validated through proper observable quantities upon perturbation of the potential parameters, which include structural, dynamical and thermodynamic properties of both LJ and

methane model systems. We stress here that the utilized SA method based on RER and the pathwise FIM is independent of the observable quantities, which is not the case for derivative-based SA methods where they suffer from smoothness assumptions on the observable functionals. The partial derivative of an observable is related with the RE through the Pinsker inequality (see ineq. (16)). The Pinsker inequality asserts that small RER (or FIM) values result in small changes in observable expectation values under perturbation; thus RER and FIM can serve as a screening tool for specific observables. The present work provides a detailed quantitative study concerning the relation between the pathwise SA method (RER / FIM tools) and specific observables of molecular systems. Specifically, it can be inferred that the parameter that controls the well's position of the LJ potential (i.e., σ_{LJ}) is two orders of magnitude more sensitive than the strength of the LJ potential (i.e., ϵ_{LJ}) in terms of RER for the LJ fluid model as well as for the methane model. This result is also confirmed by the observables. Moreover, we show that 5% perturbation of σ_{LJ} is more crucial in terms of RER (but also supported from the observable functions) than changing the potential cut-off radius from $4\sigma_{LJ}$ to $1.6\sigma_{LJ}$. Interestingly, the use of RER as an information criterion to assign values to simulation parameters such as the cutoff radius may result in accelerated MD simulations with the induced error being controlled by the RER. Finally, the intramolecular parameters (i.e., the parameters of the bonds) in the methane model are more sensitive in terms of RER than the intermolecular parameters which is explained by the fact that the bond and angle forces are stiffer than the between-atoms LJ forces.

The organization of the paper is as follows. The following Section describes the path-wise sensitivity analysis method for Langevin dynamics in detail. In Section III, the LJ fluid model, the methane model as well as various observable functions are presented followed by Section IV where the validation of the proposed pathwise SA method is demonstrated. Finally, we conclude the paper in Section V.

II. PATHWISE SENSITIVITY ANALYSIS FOR LANGEVIN DYNAMICS

This Section describes and motivates the info-theoretic approach for sensitivity analysis of stochastic Molecular Dynamics. Particularly, the RER and the corresponding pathwise FIM are derived for the Langevin equation.

A. Stochastic equation of motion

Langevin dynamics models a Hamiltonian system which is coupled with a thermostat.³² The thermostat serves as a reservoir of energy. In Langevin dynamics,

the motion of particles is governed through a probabilistic framework by a system of stochastic differential equations given by

$$\begin{cases} dq_t = M^{-1}p_t dt \\ dp_t = F^\theta(q_t)dt - \gamma M^{-1}p_t dt + \sigma dW_t, \end{cases} \quad (1)$$

where $q_t \in \mathbb{R}^{dN}$ is the position vector of the N particles in d -dimensions, $p_t \in \mathbb{R}^{dN}$ is the momentum vector of the particles, M is the (diagonal) mass matrix, $F^\theta(\cdot) : \mathbb{R}^{dN} \rightarrow \mathbb{R}^{dN}$ is the driving (conservative) force which depends on a parameter vector $\theta \in \mathbb{R}^K$ (e.g. parameters of the specific atomistic force field), γ is the friction matrix, σ is the diffusion matrix and W_t is a dN -dimensional Brownian motion. In the equilibrium regime, the forces are of gradient form, i.e., $F^\theta(q_t) = -\nabla V^\theta(q_t)$ where $V^\theta(\cdot)$ is the potential energy. Moreover, the fluctuation-dissipation theorem asserts that friction and diffusion terms are related with the inverse temperature $\beta \in \mathbb{R}$ of the system by

$$\sigma\sigma^T = 2\beta^{-1}\gamma.$$

Under gradient-type forces and the fluctuation dissipation theorem, the Langevin system has a Gibbs equilibrium (or invariant) distribution, $\mu^\theta(\cdot, \cdot)$, given by

$$\mu^\theta(dq, dp) = \frac{1}{Z} e^{-\beta(V^\theta(q) + \frac{1}{2}p^T M^{-1}p)} dq dp. \quad (2)$$

In non-equilibrium steady states, however, the stationary distribution, $\mu^\theta(\cdot, \cdot)$, is generally not known restricting the sensitivity analysis methods that rely on the explicit knowledge of the steady states. Though, as we show below, the proposed pathwise sensitivity methodology is not limited to equilibrium systems and it works equally well in the non-equilibrium steady states regime since it only necessitates the explicit knowledge of the driving forces (i.e., the local dynamics).

B. Relative Entropy Rate and Fisher Information Matrix for Langevin Processes

Let the path space \mathcal{X} be the set of all trajectories $\{(q_t, p_t)\}_{t=0}^T$ generated by the Langevin equation in the time interval $[0, T]$. Let $Q_{[0, T]}^\theta$ denote the path space distribution, i.e., the probability to see a particular element of path space, \mathcal{X} , for a specific set of parameters θ . Consider also a perturbation vector, $\epsilon_0 \in \mathbb{R}^K$, and denote by $Q_{[0, T]}^{\theta+\epsilon_0}$ the path space distribution of the perturbed process, $(\tilde{q}_t, \tilde{p}_t)$. The proposed sensitivity analysis approach is based on the quantification of the difference between the two path space probability distributions by computing the relative entropy (RE) between them. Thus, the pathwise RE of the unperturbed distribution, $Q_{[0, T]}^\theta$, with respect to (w.r.t.) the perturbed distribution, $Q_{[0, T]}^{\theta+\epsilon_0}$, assuming that they are absolutely

continuous w.r.t. each other is defined as

$$\mathcal{R}(Q_{[0, T]}^\theta | Q_{[0, T]}^{\theta+\epsilon_0}) := \int \log \left(\frac{dQ_{[0, T]}^\theta}{dQ_{[0, T]}^{\theta+\epsilon_0}} \right) dQ_{[0, T]}^\theta, \quad (3)$$

where $\frac{dQ_{[0, T]}^\theta}{dQ_{[0, T]}^{\theta+\epsilon_0}}$ is the Radon-Nikodym derivative and it is well-defined due to the absolute continuity assumption. A key property of RE is that $\mathcal{R}(Q_{[0, T]}^\theta | Q_{[0, T]}^{\theta+\epsilon_0}) \geq 0$ with equality if and only if $Q_{[0, T]}^\theta = Q_{[0, T]}^{\theta+\epsilon_0}$, which allows us to view relative entropy as a ‘‘distance’’ (more precisely a semi-metric) between two probability measures capturing the relative importance of parameter vector changes.⁸ Moreover, from an information theory perspective, the relative entropy measures *loss/change of information* when $Q_{[0, T]}^{\theta+\epsilon_0}$ is considered instead of $Q_{[0, T]}^\theta$.³³

The necessary and sufficient conditions of the two path distributions (perturbed and unperturbed) to be absolutely continuous are provided next.

Assumption II.1. *Assume that*

(a) *the diffusion matrix, σ , is invertible, and,*

(b) $\mathbb{E}_{Q_{[0, T]}^\theta} [\exp \{ \int_0^T |u(q_t, p_t)|^2 dt \}] < \infty$, *where the function $u(\cdot, \cdot) : \mathbb{R}^{2dN} \rightarrow \mathbb{R}^{2dN}$ is defined such that for all pairs (q, p) it should hold that*

$$\begin{bmatrix} 0 & 0 \\ 0 & \sigma \end{bmatrix} u(q, p) = \begin{bmatrix} M^{-1}p - M^{-1}p \\ F^\theta(q) - \gamma M^{-1}p - (F^{\theta+\epsilon_0}(q) - \gamma M^{-1}p) \end{bmatrix},$$

or, equivalently,

$$\begin{bmatrix} 0 \\ \sigma \end{bmatrix} u(q, p) = \begin{bmatrix} 0 \\ F^\theta(q) - F^{\theta+\epsilon_0}(q) \end{bmatrix}.$$

Notice that such a function, $u(\cdot, \cdot)$, exists due to (a). Furthermore, (a) implies that the noise is non-degenerate for the momenta. Then, the RE of the path distribution defined in (3) is finite and an explicit formula can be estimated as the following proposition asserts.

Proposition II.1. *Let Assumption II.1 holds. Assume also that $(q_0, p_0) \sim \nu^\theta$ and $(\tilde{q}_0, \tilde{p}_0) \sim \nu^{\theta+\epsilon_0}$ where $\nu^\theta(\cdot, \cdot)$ and $\nu^{\theta+\epsilon_0}(\cdot, \cdot)$ are two initial distributions which should be absolutely continuous w.r.t. each other. Then,*

$$\begin{aligned} \mathcal{R}(Q_{[0, T]}^\theta | Q_{[0, T]}^{\theta+\epsilon_0}) &= \mathcal{R}(\nu^\theta | \nu^{\theta+\epsilon_0}) \\ &+ \frac{1}{2} \mathbb{E}_{Q_{[0, T]}^\theta} \left[\int_0^T |u(q_t, p_t)|^2 dt \right] \end{aligned} \quad (4)$$

Proof. Under Assumption II.1, the Girsanov theorem applies providing an explicit formula of the Radon-Nikodym derivative³⁴ which is given by

$$\begin{aligned} \frac{dQ_{[0, T]}^\theta}{dQ_{[0, T]}^{\theta+\epsilon_0}} \left(\{(q_t, p_t)\}_{t=0}^T \right) &= \frac{d\nu^\theta}{d\nu^{\theta+\epsilon_0}}(q_0, p_0) \times \\ \exp \left\{ - \int_0^T u(q_t, p_t)^T dW_t - \frac{1}{2} \int_0^T |u(q_t, p_t)|^2 dt \right\}. \end{aligned}$$

Moreover, $\hat{W}_t := \int_0^t u(q_s, p_s) dt + W_t$ is a Brownian motion with respect to the path distribution $Q_{[0,T]}^\theta$, meaning that, for any measurable function $f(\cdot, \cdot)$, it holds $\mathbb{E}_{Q_{[0,T]}^\theta} [\int_0^T f(q_t, p_t)^T d\hat{W}_t] = 0$. Then,

$$\begin{aligned} \mathcal{R}(Q_{[0,T]}^\theta | Q_{[0,T]}^{\theta+\epsilon_0}) &= \int \left(\log \frac{d\nu^\theta}{d\nu^{\theta+\epsilon_0}}(q_0, p_0) \right. \\ &\quad \left. - \int_0^T u(q_t, p_t)^T dW_t - \frac{1}{2} \int_0^T |u(q_t, p_t)|^2 dt \right) dQ_{[0,T]}^\theta \\ &= \int \log \frac{d\nu^\theta}{d\nu^{\theta+\epsilon_0}}(q_0, p_0) dQ_{[0,T]}^\theta - \int \int_0^T u(q_t, p_t)^T d\hat{W}_t dQ_{[0,T]}^\theta \\ &\quad + \frac{1}{2} \int \int_0^T |u(q_t, p_t)|^2 dt dQ_{[0,T]}^\theta \\ &= \mathcal{R}(\nu^\theta | \nu^{\theta+\epsilon_0}) + \frac{1}{2} \int \int_0^T |u(q_t, p_t)|^2 dt dQ_{[0,T]}^\theta \end{aligned}$$

□

We remark that this proposition is a result on the transient regime since the initial distributions can be anything as far as they are absolutely continuous w.r.t. each other. In the stationary regime, a significant simplification of the pathwise RE occurs. As the following proposition asserts, pathwise RE is decomposed into a linear in time term plus a constant where the slope of the linear term is the relative entropy rate (RER).

Proposition II.2. *Let Assumption II.1 holds. Assume also that $(q_0, p_0) \sim \mu^\theta$ and $(\bar{q}_0, \bar{p}_0) \sim \mu^{\theta+\epsilon_0}$ where $\mu^\theta(\cdot, \cdot)$ and $\mu^{\theta+\epsilon_0}(\cdot, \cdot)$ are the stationary distributions for the unperturbed and the perturbed process, respectively, which should be absolutely continuous w.r.t. each other. Then, the pathwise RE equals to*

$$\mathcal{R}(Q_{[0,T]}^\theta | Q_{[0,T]}^{\theta+\epsilon_0}) = T\mathcal{H}(Q^\theta | Q^{\theta+\epsilon_0}) + \mathcal{R}(\mu^\theta | \mu^{\theta+\epsilon_0}) \quad (5)$$

where

$$\begin{aligned} \mathcal{H}(Q^\theta | Q^{\theta+\epsilon_0}) &:= \\ &\frac{1}{2} \mathbb{E}_{\mu^\theta} [(F^{\theta+\epsilon_0}(q) - F^\theta(q))^T (\sigma\sigma^T)^{-1} (F^{\theta+\epsilon_0}(q) - F^\theta(q))] \end{aligned} \quad (6)$$

is the Relative Entropy Rate.

Proof. First notice that we drop the T subscript from the definition of RER because RER is time-independent. Then, it is straightforward to show from the previous proposition that

$$\begin{aligned} \mathcal{R}(Q_{[0,T]}^\theta | Q_{[0,T]}^{\theta+\epsilon_0}) &= \mathcal{R}(\mu^\theta | \mu^{\theta+\epsilon_0}) + \frac{1}{2} \int \int_0^T |u(q_t, p_t)|^2 dt dQ_{[0,T]}^\theta \\ &= \mathcal{R}(\mu^\theta | \mu^{\theta+\epsilon_0}) + \frac{1}{2} \int_0^T \int |u(q_t, p_t)|^2 dQ_{[0,T]}^\theta dt \\ &= \mathcal{R}(\mu^\theta | \mu^{\theta+\epsilon_0}) + \frac{1}{2} \int_0^T \int |u(q, p)|^2 \mu^\theta(dq, dp) dt \\ &= \mathcal{R}(\mu^\theta | \mu^{\theta+\epsilon_0}) + \frac{T}{2} \mathbb{E}_{\mu^\theta} [|u(q, p)|^2]. \end{aligned}$$

□

RER inherits all the properties of relative entropy (non-negativity, convexity, etc.) and it measures the change of information in path space per unit time. For large times, the term that involves RER is the significant term, since it scales linearly with time, while the constant one becomes less and less important. Moreover, the estimation of RER necessitates only the knowledge of the driving forces (i.e., the local dynamics) which is available since the driving forces are computed in any numerical scheme of the Langevin equation.

Pathwise Fisher information matrix: Generally, RE is locally a quadratic functional in a neighborhood of parameter vector, θ . Under smoothness assumption in the parameter vector, the curvature of the RE around θ , defined by its Hessian, is the FIM. Analogously, we define the Hessian of the RER to be the pathwise FIM denoted by $F_{\mathcal{H}}(Q^\theta)$. The relation between the RER and the pathwise FIM is

$$\mathcal{H}(Q^\theta | Q^{\theta+\epsilon_0}) = \frac{1}{2} \epsilon_0^T F_{\mathcal{H}}(Q^\theta) \epsilon_0 + \mathcal{O}(|\epsilon_0|^3). \quad (7)$$

Under smoothness assumption of the force vector, $F^\theta(\cdot)$, w.r.t. to the parameter vector, θ , an explicit formula for the pathwise FIM for the Langevin process is straightforwardly obtained from (6) given by

$$F_{\mathcal{H}}(Q) = \mathbb{E}_{\mu^\theta} [\nabla_\theta F^\theta(q)^T (\sigma\sigma^T)^{-1} \nabla_\theta F^\theta(q)], \quad (8)$$

where $\nabla_\theta F^\theta(\cdot)$ is a $dN \times K$ matrix containing all the first-order partial derivatives of the force vector (i.e., the Jacobian matrix). Observe that the pathwise FIM does not depend on the perturbation vector, ϵ_0 , making pathwise FIM an attractive “gradient-free” quantity for sensitivity analysis. Indeed, the RER for any perturbation can be recovered up to third-order utilizing only the pathwise FIM and (7). Moreover, the spectral analysis of $F_{\mathcal{H}}(Q)$ would allow to identify which parameter directions are most/least sensitive to perturbations.

Example 1: Unknown stationary distribution:

In many molecular systems the steady state is not a Gibbs distribution and typically it is not known explicitly. This is commonplace in non-equilibrium molecular systems such as models with multiple mechanisms, e.g. reaction-diffusion systems, or driven molecular systems.^{25,35} Here we consider such a mathematically simple example, where we assume that the force field consists of two components; one conservative term given as minus the gradient of the potential energy and another term that is not the gradient of a potential function. Mathematically, the force field is given by

$$F^\theta(q) = -\nabla V^\theta(q) + G(q)$$

where we further assume for simplicity that only the conservative term depends on the parameter vector, θ . Since, the resulting Langevin process is at the non-equilibrium regime, the steady states do not admit an explicit form.

However, denoting by $\bar{\mu}^\theta$ the unknown stationary distribution of the Langevin process driven by the above forces, the RER is given by

$$\mathcal{H}(Q^\theta|Q^{\theta+\epsilon_0}) = \frac{1}{2}\mathbb{E}_{\bar{\mu}^\theta}[(\nabla V^{\theta+\epsilon_0}(q) - \nabla V^\theta(q))^T(\sigma\sigma^T)^{-1}(\nabla V^{\theta+\epsilon_0}(q) - \nabla V^\theta(q))] . \quad (9)$$

Notice that the expression in the expectation does not depend on the non-conservative forces and it is the same expression as in the equilibrium regime. However, the dependence on the non-conservative forces is evident through the (unknown) stationary distribution, $\bar{\mu}^\theta$.

Example 2: Inverse temperature perturbation: Using the fluctuation-dissipation relation, we can substitute the friction parameter γ with the inverse temperature β and compute the RER and the pathwise FIM for β perturbations. Indeed, substituting in eq. (6) the relation $\gamma = \frac{1}{2}\beta\sigma\sigma^T$, we are looking for $u(\cdot, \cdot)$ such that

$$\begin{bmatrix} 0 & 0 \\ 0 & \sigma \end{bmatrix} u(q, p) = \begin{bmatrix} 0 \\ -\frac{1}{2}\beta\sigma\sigma^T M^{-1}p + \frac{1}{2}(\beta + \epsilon_\beta)\sigma\sigma^T M^{-1}p \end{bmatrix} ,$$

where ϵ_β is the perturbation of inverse temperature. Notice that the forces were cancelled out in this expression for u because no perturbation is performed in the parameters of the forces. At the stationary regime, RER is then given by

$$\mathcal{H}(Q^\beta|Q^{\beta+\epsilon_\beta}) = \frac{\epsilon_\beta^2}{8}\mathbb{E}_{\mu^\beta}[p^T M^{-1}\sigma\sigma^T M^{-1}p] , \quad (10)$$

where $\mu^\beta(\cdot)$ is the stationary distribution of the process. It is evident that RER is a quadratic function of the perturbation of the inverse temperature and interestingly enough it depends only on the momenta, p . The above formula is valid for any force field and implies that the sensitivity of the (inverse) temperature as quantified by the relative entropy between path distributions is independent of the underlying system as it defined by the forces or by the potential function, $V^\theta(\cdot)$.

Furthermore, in the equilibrium regime where the stationary distribution is given by the Gibbs measure (eq. (2)), (10) can be further simplified because of the Gaussian nature of the momenta, p . Indeed, assuming for simplicity that $M = mI_{dN}$ and $\sigma = \sigma I_{dN}$ with $m, \sigma \in \mathbb{R}$, (10) is rewritten as

$$\mathcal{H}(Q^\beta|Q^{\beta+\epsilon_\beta}) = \frac{\epsilon_\beta^2\sigma^2}{8\beta m}dN . \quad (11)$$

Consequently, the pathwise FIM in the logarithmic scale (see equation below) is given by

$$F_{\mathcal{H}}(Q^{\log\beta}) = \frac{\gamma}{2m}dN . \quad (12)$$

SA in the logarithmic scale: In many molecular systems, the model parameters may differ by orders of magnitude, thus, it is more appropriate to perform relative perturbations, i.e., the i -th element of the perturbation

vector is $\theta_i\epsilon_{0,i}$. After straightforward algebra, the elements of the logarithmic-scale Fisher information matrix are given by

$$(F_{\mathcal{H}}(Q^{\log\theta}))_{i,j} = \theta_i\theta_j(F_{\mathcal{H}}(Q^\theta))_{i,j} , \quad i, j = 1, \dots, K . \quad (13)$$

We refer to Ref. 12 for more details.

Statistical estimators: Even though the Langevin equation is degenerate since the noise applies only to the momenta, the process is hypo-elliptic and ergodic under mild conditions on the potential energy, $V(\cdot)$. Therefore, RER and the corresponding pathwise FIM can be computed as ergodic averages. Note though that in order to obtain samples from the Langevin process, a numerical scheme should be employed resulting in errors due to the discretization procedure. There exist several numerical integrators such as BBK and BAOAB for the Langevin equation.^{32,36} In Appendix A, BBK integrator is briefly reviewed. The inserted bias is of order $O(\Delta t)$ where Δt is the time-step as it has been shown for Langevin equation under compactness condition³⁷⁻³⁹ (e.g., under bounded domain). Then, the statistical estimator for the RER is given by

$$\bar{\mathcal{H}}(Q^\theta|Q^{\theta+\epsilon_0}) = \frac{1}{2n} \sum_{i=1}^n (F^{\theta+\epsilon_0}(q^{(i)}) - F^\theta(q^{(i)}))^T (\sigma\sigma^T)^{-1} (F^{\theta+\epsilon_0}(q^{(i)}) - F^\theta(q^{(i)})) , \quad (14)$$

where n is the number of samples and, similarly, the statistical estimator for the pathwise FIM is given by

$$\bar{F}_{\mathcal{H}}(Q^\theta) = \frac{1}{n} \sum_{i=1}^n \nabla_\theta F^\theta(q^{(i)})^T (\sigma\sigma^T)^{-1} \nabla_\theta F^\theta(q^{(i)}) . \quad (15)$$

Sensitivity Bound: Relative entropy provides a mathematically elegant and computationally tractable methodology for the parameter sensitivity analysis of Langevin systems. Such an approach focuses on the sensitivity of the entire probability distribution, either at equilibrium or at the path-space level, i.e., for the entire stationary time-series quantifying among others the transferability skills of the molecular models. However, in many situations in molecular simulations, the interest is focused on observables such as radial distribution function, pressure, mean square displacement, etc. Therefore, it is desirable to attempt to connect the parameter sensitivities of observables to the relative entropy methods proposed here. Indeed, relative entropy can provide an upper bound for a large family of observable functions, g , through the Pinsker (or Csiszar-Kullback-Pinsker) inequality,³³

$$|\mathbb{E}_{Q_{[0,T]}^{\theta+\epsilon_0}}[g] - \mathbb{E}_{Q_{[0,T]}^\theta}[g]| \leq \|g\|_\infty \sqrt{2\mathcal{R}(Q_{[0,T]}^\theta|Q_{[0,T]}^{\theta+\epsilon_0})} \quad (16)$$

where $\|\cdot\|_\infty$ denotes the supremum (here, maximum) of g . In the context of sensitivity analysis, inequality (16) states that if the relative entropy is small, i.e., insensitive in a particular parameter direction, then, any bounded observable g is also expected to be insensitive towards the same direction. In this sense, ineq. (16) can be viewed as a screening tool for parametric "insensitivity analysis" of observables. Sensitivity bounds sharper than ineq. (16)

are also being developed.⁴⁰ Note that the inverse is not justified; i.e. if the relative entropy is large for a specific parameter direction, then an observable g might, or might not, exhibit sensitivity with respect to the same parameter direction.

III. MODELS AND OBSERVABLES

This section describes the two molecular models discussed here and several observable functions on which the proposed sensitivity analysis method is validated. A prototypical Lennard-Jones fluid model with two force field parameters and a methane model with ten parameters are presented. Observables such as the radial distribution function, the mean square displacement and the pressure spanning from a wide range of model properties are also provided. All simulations are performed under constant number of atoms, volume and temperature (NVT ensemble).

A. LJ fluid model

In order to investigate the sensitivity analysis for a realistic system we examine the LJ fluid model. In this model, the atoms are identical, interacting with the Lennard Jones potential with reduced non-dimensional parameters $\epsilon_{LJ} = 1, \sigma_{LJ} = 1$. One of the advantages of the LJ fluid is that there exists a phase diagram of the reduced density ρ^* versus the reduced temperature T^* .³⁰ The popularity of this model relies on the generality of systems of molecular liquids that can be described as well as computational efficiency. We restrict the force field interactions in the vicinity of cutoff radius r_{cut} . Thus, the (truncated) LJ pair potential is given by

$$V_{LJ}(r_{ij}) = \begin{cases} 4\epsilon_{LJ} \left[\left(\frac{\sigma_{LJ}}{r_{ij}} \right)^{12} - \left(\frac{\sigma_{LJ}}{r_{ij}} \right)^6 \right], & \text{if } r_{ij} < r_{cut} \\ 0, & \text{otherwise,} \end{cases} \quad (17)$$

while the total potential energy of the system is

$$V_{LJ}(q) = \sum_{\substack{1 \leq i, j \leq N \\ i < j}} V_{LJ}(r_{ij}),$$

with

$$r_{ij} = |q_i - q_j| = \sqrt{(q_i^x - q_j^x)^2 + (q_i^y - q_j^y)^2 + (q_i^z - q_j^z)^2},$$

being the Euclidean distance between the atoms.

Sensitivity analysis is performed on the LJ potential parameters ϵ_{LJ} and σ_{LJ} and as we show later (see section IV), the most sensitive parameter is the latter. We consider a system of $N = 2048$ atoms in a cubic simulation box of side length $L = 14.3\sigma_{LJ}$ with periodic boundary conditions (PBC). The reduced temperature of the

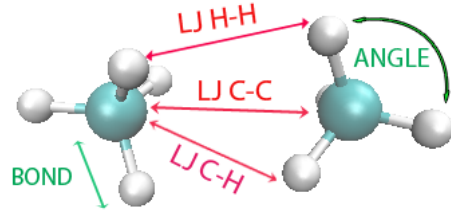


Figure 1. Visualization of the CH_4 interactions. The site site non-bonded LJ interactions (intermolecular) are marked in red whereas the intramolecular potential interactions are marked in green.

run is $T^* = 0.85\tau$ which means that the system is in liquid phase (number density $\rho^* = 0.7$). For the numerical scheme, the time-step is $\Delta t = 10^{-3}$ while the length of the run is 10^5 time-steps. An equilibration period of 10^4 steps is sufficient for the fcc lattice to melt and standard reduced units are used throughout the simulations.

B. CH_4 model

Methane is a more complicated molecule combined of two different types of atoms; carbon (C) and hydrogen (H). Active research is targeted on CH_4 because of its environmental impact and energy utilization.⁴¹ Our sensitivity study is expanded and validated on this more complex molecular model which consists of different intermolecular potentials between the pairs of atoms (bonded and non-bonded) as well as additional parameters imposed by the geometry of the molecule (bonds and angles). We define $V(q)$ the total potential and N the total number of atoms (both C's and H's).

$$V(q) = V_{bond}(q) + V_{angle}(q) + V_{LJ}(q). \quad (18)$$

where $V_{bond}(q), V_{angle}(q)$ are quadratic intramolecular potential functions of the bonds and angles respectively. $V_{LJ}(q)$ is the non-bonded potential as defined in the previous subsection. For more details concerning the model see Appendix C.

The parameter vector, θ , consists of six LJ parameters (three different LJ potentials depending on the atom type, see also Figure 1), two bond parameters and two angle parameters. The parameters values of CH_4 are summarized in Table I whereas the values of the simulation parameters are presented in Table II.

C. Observables

To validate the proposed pathwise SA approach we have calculated various observables that are related to thermodynamical, structural and dynamical properties of

	$\epsilon_{LJ} [\frac{Kcal}{mol}]$	$\sigma_{LJ} [\text{\AA}]$	$r_{cut} [\text{\AA}]$
$C - C$	0.0951	3.473	15.0
$C - H$	0.0380	3.159	15.0
$H - H$	0.0152	2.846	15.0
$K_b [\frac{Kcal}{mol\text{\AA}^2}]$	$r_0 [\text{\AA}]$	$K_\theta [\frac{Kcal}{mol\cdot deg^2}]$	$\theta_0 [\text{rad}]$
700	1.1	100	1.909

Table I. Non-bonded LJ coefficients as well as bond and angle coefficients for methane.³¹

N(molecules)	T [K]	L [\AA]	$\rho [\frac{mols}{\text{\AA}^3}]$	γ
512	100	32.9	0.0143	0.5

Table II. Simulation parameters for CH_4

the molecular stochastic models. These quantities are experimentally tractable and are related to the microscopic as well as the macroscopic level. In more detail, here, we focus on radial distribution function (RDF), mean square displacement (MSD) and pressure. Other studies²³ in the literature computed observables such as the Helmholtz free energy, density, enthalpy to name some. Despite the fact that the RDF as well as the pressure are equilibrium quantities, MSD is related to the dynamics (time-series averaging) making the proposed pathwise method suitable for such long-time quantities. Note also, that there are no closed analytic expressions for all the above observables with respect to the force field (model) parameters.

1. Radial distribution function

The structure of liquids is characterized by the pair radial distribution function, $g(r)$, ($g^{(2)}(r)$ to be more precise) and it is the most important observable of molecular simulations due to the fact that the ensemble average of any pair function may be expressed by it.^{1,42} Furthermore, $g(r)$ can be calculated experimentally by X-ray diffraction.⁴² The RDF is the pair distribution function that indicates the normalized distribution of a pair of identical atoms (or molecules) at a given distance. For long intermolecular distance r in liquids, $g(r)$ fluctuates around unity. This static observable is based on the equilibrium structure of the system and it is constructed by histogram averages. For N identical atoms let the two-atom distribution function be

$$P_N^{(2)}(q_1, q_2) := \frac{1}{(N-2)!} \int e^{-\beta V(\mathbf{q})} dq_3 \dots dq_N, \quad (19)$$

where q_1, q_2 are the positions of the first and second atoms kept fixed, irrespective of the configuration of the rest of the particles. For a (homogeneous) liquid, it holds that

$$P_N^{(2)} = \rho^2 g^{(2)}(|r_{1,2}|), \quad \rho = \frac{N}{\text{Vol}} \quad (20)$$

where ρ is the number density while Vol is the volume of the simulation box. If the atoms were independent of each other, $P^{(2)}$ would equal ρ^2 so in practice $g(r)$ corrects for the spatial (density) correlation between atoms. For the CH_4 model, we consider the molecular $g(r)$ which is based on the center of mass of each individual molecules.

2. Mean square displacement

The mean square displacement associates the diffusion coefficient, D , with the atom (or center of mass for molecules) coordinates and is a measure of the spatial extent of random motion of the Langevin dynamics. It is defined as

$$MSD = \langle (q_t - q_{t_0})^2 \rangle = \mathbb{E}_{Q_{[t_0, t]}} [(q_t - q_{t_0})^2] \quad (21)$$

where q_t, q_{t_0} are vectors of particle positions at time t and reference time instant t_0 , while the brackets, $\langle \cdot, \cdot \rangle$, denote ensemble averaging over all configurations of all the atoms (or molecules). This quantity provides us with information about the dynamical properties of the system. The MSD and the diffusion coefficient, D , are related by Einstein's equation

$$2D = \frac{1}{d} \lim_{t \rightarrow \infty} \frac{\partial \langle (q_t - q_{t_0})^2 \rangle}{\partial t} \quad (22)$$

Where d is the dimension of the system (here $d = 3$).

3. Pressure

Temperature and pressure are macroscopic thermodynamic parameters defined in an experimental setup but they can also be defined microscopically. Pressure is given by the expression¹

$$P = \frac{\rho}{\beta} + \frac{vir}{\text{Vol}},$$

where the first term is the kinetic energy contribution while vir is the atomic (or molecular) virial given by

$$vir = \frac{1}{3} \sum_{1 \leq i \leq N} \sum_{j > i} F_{ij} r_{ij}.$$

Note that F_{ij} is the total force (both non-bonded and bonded in the CH_4 case) between atoms (or molecules) i and j .

IV. RESULTS

Every model at hand has a domain of applicability; i.e., the forcefield representation allows to calculate (usually thermodynamic) properties of interest in accordance to

experimental values within a margin of error. This means that a force field might represent well one property, such as density, but may not be valid for others, or might represent all of them less accurately. In the following we perform simulations where the RER and FIM for each perturbed variable are computed. Discussion on the results as well as validation with respect to the observable quantities defined in section III C supports our results.

A. LJ fluid

RER and FIM calculations for the LJ fluid are summarized in Figure 2. We compare the RER value using the continuous time statistical estimators, Eqs. 14, 15. The middle bar corresponds to the FIM-based RER whereas the left and right bars are the values of estimator 14 for a negative and positive perturbation by $\epsilon_0 = 5\%$ respectively. All the plots are normalized upon division with the number of particles. As the figure suggests σ_{LJ} is the most sensitive parameter. Systems size effects have been thoroughly examined by performing test simulations of bigger systems under the same parameters, which produce similar results to those presented here. It has been shown for a similar model that uncertainty in thermodynamic and transport properties based on the potential parameters is larger than statistical simulation uncertainty.⁹

The corresponding results for the discrete time case using the BBK integrator are shown in the Appendix. There's minor discrepancy of order $O(\Delta t)$ as previously mentioned in section II due to the discretization error bias. We note here that the continuous time computations are faster since the RER and FIM formulas are less complex.

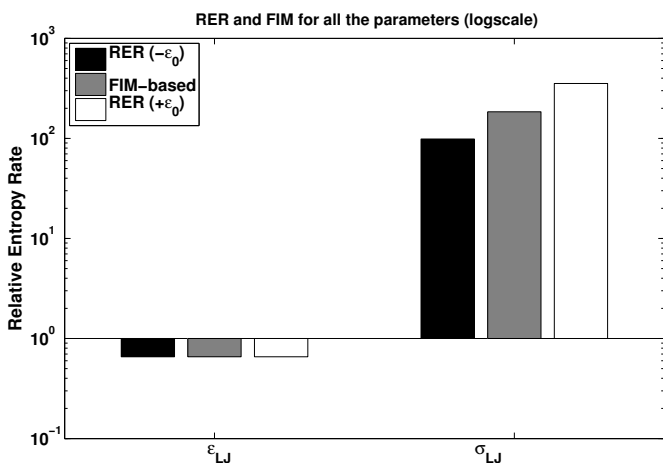


Figure 2. RER and FIM of continuous time estimators (14), (15). Comparing with the discrete time case (supplementary material), the values are almost identical. σ_{LJ} is the most sensitive parameter.

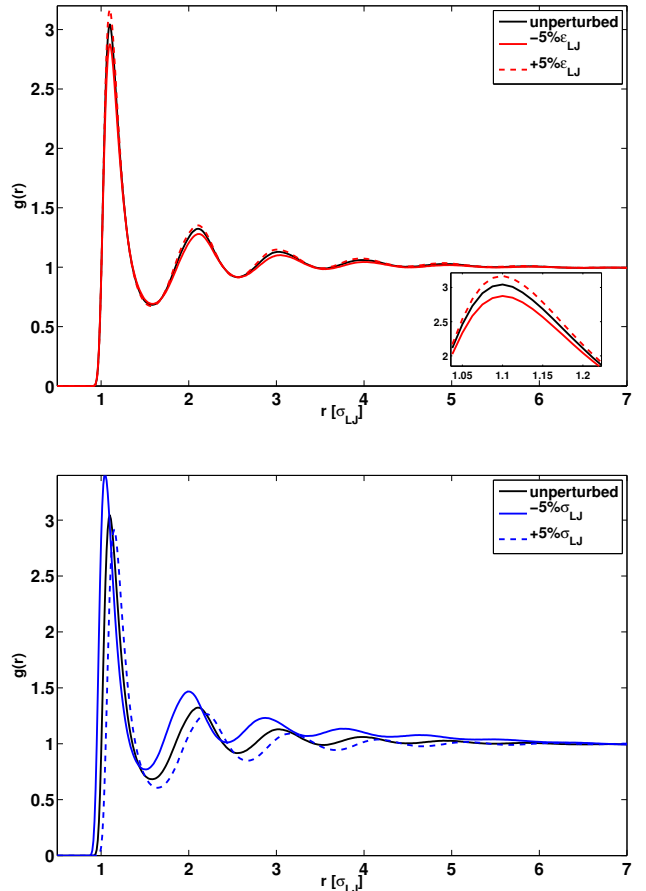


Figure 3. Effect of perturbation of ϵ_{LJ} parameter by $\pm 5\%$ (upper panel) and σ_{LJ} parameter by $\pm 5\%$ (lower panel) on RDF. The first peak is shifted vertically for fluctuations around ϵ_{LJ} whereas it is shifted to the right or left when the fluctuations concern the σ_{LJ} parameter. It is clear that σ_{LJ} (lower panel) is more sensitive as the plots differ substantially, which is in agreement with the RE method.

perturbation	$\ g^\theta(r) - g^{\theta+\epsilon_0}(r)\ _{L_2}$	$\frac{ g^\theta - g^{\theta+\epsilon_0} }{ g^\theta }$	RER
+5% ϵ_{LJ}	0.049	0.8 %	0.79
-5% ϵ_{LJ}	0.066	-1.17%	0.79
+5% σ_{LJ}	0.47	-3.83 %	409
-5% σ_{LJ}	0.59	7.4 %	115
$r_{cut} = 1.6\sigma_{LJ}$	0.189	-3.44 %	0.71
$r_{cut} = 7\sigma_{LJ}$	0.01	0.19%	1.6×10^{-4}

Table III. L_2 norm of the difference of the unperturbed minus the perturbed $g(r)$ and normalized area difference.

Validation on the stronger sensitivity on σ_{LJ} compared to ϵ_{LJ} , is demonstrated by the RDF ($g(r)$) plots shown in Figure 3. Note that the gradient of the potential, i.e. the interatomic force, depends linearly with respect to ϵ_{LJ} . An increase in this parameter leads to a deeper potential well and stronger attraction between the atoms at the

same distance. Thus, as expected, positive perturbation in ϵ_{LJ} leads to an increase of the first peak in the RDF graph. In addition, only the first peak of the $g(r)$ is affected, the rest of the curve remains the same. Positive (negative) perturbations on the σ_{LJ} parameter shift the whole RDF graph due to the fact that the atoms sense greater (weaker) repulsion forces. Hence, the distribution maximum is transferred to a longer (shorter) distance. We also notice that the peak of the curve has increased at the new maximum which can be explained by the finite volume of the same simulation box (NVT ensemble) of the unperturbed system.

In order to get a more detailed insight on the RDFs shown in Figure 3 we have also computed the L_2 norm, shown in Table III. The L_2 norm is suitable for a comparison of the unperturbed versus the perturbed plots $g^\theta(r)$ and $g^{\theta+\epsilon_0}(r)$ respectively. As the RER/FIM computations have shown that there is a relative entropy difference of about 2 orders of magnitude with respect to the two potential parameters (Figure 2), we now observe a consistent difference, of about 5 times in L_2 , for the RDF observable. Table III and Figure 3 suggest that the positively and negatively perturbed RDF plots exhibit a more symmetric behavior on the ϵ_{LJ} parameter than the σ_{LJ} . Moreover $-5\%\sigma_{LJ}$ changes the packing of the LJ fluid completely; all the density distribution peaks are moved to a shorter distance. This result is consistent with Pinsker’s inequality (16) as the more sensitive direction allows for greater differences in the expected values of the observables.

Opposite perturbation directions yield different RER values whereas this is not the case for the FIM based RER which is a second-order (quadratic) approximation. In one of the realizations in our example, RER for $+(-)5\%\sigma_{LJ}$ is 360.7 (101.1) and FIM is 196.6 meaning that $\mathcal{H}(Q^\theta|Q^{\theta\pm\epsilon_0})$ is not symmetric w.r.t. FIM and the negative direction being more sensitive.

There is no analytic formula that relates the MSD to the potential parameters but we expect that a larger deviation will result upon perturbation of a more sensitive parameter. As we can see in Figure 4, the line for the insensitive perturbed parameter ϵ_{LJ} slightly differs from the black one, both for positive and negative ϵ_0 . On the contrary, the line that corresponds to the increased σ_{LJ} is further away and under the unperturbed one. Based on the aforementioned discussion on $g(r)$ this is reasonable, as an increase in the σ_{LJ} values leads to stronger repulsive forces at the same distance, hence more atom collisions and consequently to a larger friction coefficient, i.e. lower mobility of the LJ atoms. A decrease in σ_{LJ} lowers the interatomic repulsive forces and there’s no significant effect at this density because the random forcing dominates the dynamics. This result is consistent with Pinsker’s inequality as it provides an upper bound only, meaning that although this parameter is indicated as more sensitive (bigger RER value on the r.h.s.) the expected value w.r.t. this observable slightly changes upon perturbation. Additional runs (realizations

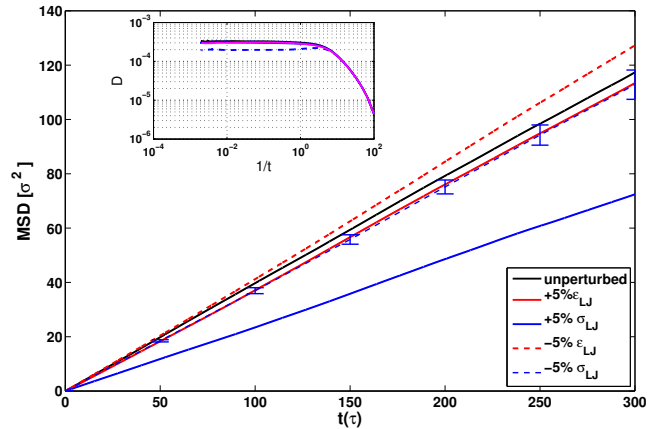


Figure 4. MSD for different perturbed directions by $\pm 5\%$. The ϵ_{LJ} parameter has a small impact in comparison with the more sensitive σ_{LJ} . The MSD plot for the positive perturbation of σ_{LJ} stands out as the increased collisions dominate the random forcing. Errorbars indicate the standard deviation for the $-5\%\sigma_{LJ}$ and the deviation propagates with time. The inset illustrates the diffusion coefficient difference in logscale.

of the Markov chain starting from different configurations) for the same negative σ_{LJ} direction have shown that the errorbars are within 2.5%. The linear dependence of the interatomic forces with respect to ϵ_{LJ} accounts for increased (decreased) interatomic interaction strength when this parameter is changed upwards (downwards).

Table IV contains the diffusion coefficient D (from eq. 22) related to Figure 4 and depicts a quantitative aspect. The perturbation direction of $+5\%\sigma_{LJ}$ is dominant and clearly results in slowing down the diffusion of the LJ fluid particles.

As mentioned above for simulation of the LJ fluid standard non-dimensional (reduced units) are used. The reduced pressure is denoted by P^* and Table IV contains the simulation results. Once more we observe a greater influence in perturbation of the parameter σ_{LJ} especially for a positive increase. This is consistent with the fact that the volume remains unchanged and the repulsive forces increase as discussed earlier, giving a pressure rise of fourteen times more for a $+5\%$ perturbation. We observe the opposite fact for a reduction in σ_{LJ} . The ϵ_{LJ} parameter has a more symmetric influence and this is explained by the linear increase in the forces (derivative of the potential formula) between the atoms and consequently via the virial coefficient it is depicted at the pressure. The third column of Table IV compares the relative pressure change with respect to the unperturbed run and the pressure standard deviation is on the column that follows. Parameter σ_{LJ} alters the pressure by an order of magnitude, a result which is consistent with the RER/FIM calculations in the previous subsection.

1. Discontinuous model parameter: cutoff radius

The r_{cut} is a parameter of the model but the potential is not differentiable with respect to it. Hence we can compute the relative entropy rate but we cannot have an estimate of the Fisher Information matrix because the computation of FIM involves products of partial derivatives (see also Eq. 15). Figure 5 summarizes the quantity $\mathcal{R}(r_{cut}^{ref}|r_{cut})$ per particle, where in this notation we mean that the RER integral differential is w.r.t. the path space measure corresponding to the model's r_{cut} as reference. The potential tends to zero at distance $r_{cut} = 2.5\sigma_{LJ}$, that is a typical value also used in the literature, so information lost upon trimming the potential tail is small in comparison to that when r_{cut} is shifted to the left. We expected that the RER should be higher for a negative perturbation of r_{cut} as validated in Figure 5 and the asymmetry (exponential form for negative perturbation) comes from the formula (plot) of the potential; more information regarding the attractive part is lost rapidly for a -10% reduction step from the reference $r_{cut} = 4\sigma_{LJ}$. Indeed the trick of the r_{cut} convention has been used in molecular simulations in order to reduce the computations at the expense of minimal information loss, so our results using this pseudo-metric indicate that our choice of r_{cut} is suitable. Additional runs for an increase in r_{cut} suggest a trivial gain of information based on the $\mathcal{H}(Q^{r_{cut}^{ref}}|Q^{r_{cut}})$ value as well as the RDF (see next).

The RDF plot changes with a change in r_{cut} as shown in Figure 6. When the potential tail is restricted up to r_{cut} , the long-range attractive part is zero after that distance. This results to weaker long-range attractive forces (loss of cohesive energy) hence the first peak in the RDF graph is lower and the mass is distributed to the right. We have included the plot of a 60% decrease to illustrate the higher dependence on a ‘‘premature’’ truncation and a plot of 75% increase for comparison. The empirical value of $2.5\sigma_{LJ}$ is adequate for simulations, but a further reduction to $1.6\sigma_{LJ}$ results to huge loss of information, especially for the attractive part. On the contrary, if we almost double the reference value of $4\sigma_{LJ}$ to $7\sigma_{LJ}$, the

perturbation	P^*	$\frac{P_{\theta^*+\epsilon_0}^* - P_{\theta^*}^*}{ P_{\theta^*}^* }$	σ_{STD}	$D[\frac{\sigma_{LJ}^2}{\tau}]$
unperturbed	0.11	-	0.25	3.2×10^{-4}
+5% ϵ_{LJ}	-0.10	-1.92	0.26	2.9×10^{-4}
-5% ϵ_{LJ}	0.28	1.56	0.23	3.4×10^{-4}
+5% σ_{LJ}	1.71	14.34	0.6	1.8×10^{-4}
-5% σ_{LJ}	-0.47	-5.24	0.12	3.04×10^{-4}

Table IV. (left) Pressure change with respect to different perturbation directions of the LJ fluid parameters. σ_{LJ} is the most sensitive direction. (right) Diffusion coefficient of the MSD plots. The errorbars are within $\pm 2.5\%$.

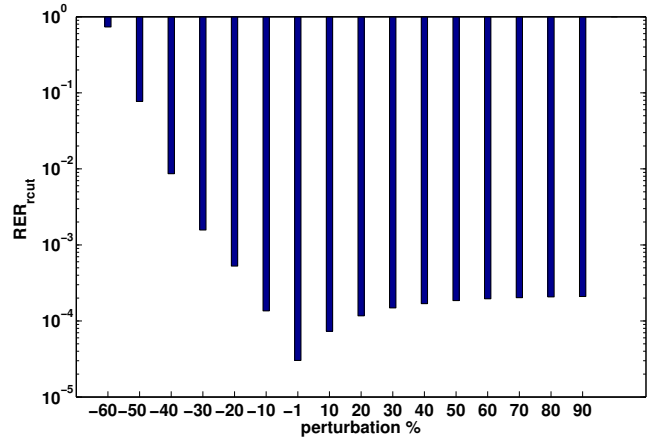


Figure 5. RER per particle for different r_{cut} values in logscale. Perturbation of -10% corresponds to the 90% of the reference $r_{cut} = 4\sigma_{LJ}$. There is significant loss of information when we restrict the potential tail (r_{cut}) to less than one half, as that value is near the minimum of the potential well and a fraction of the attractive forces is lost.

gain is minimal and this can be seen in Figures 5 and 6.

We have seen here that the influence of this parameter is minimal in comparison with the potential parameters in Figure 2 for this reference value in terms of RER. RER per parcticle for a $-5\%\epsilon_{LJ}$ perturbation is similar to a -60% reduction in r_{cut} . The L_2 norm of the $g(r)$ difference for different r_{cut} values (Table III and Figure 6) illustrate the same behavior too. At this point we should stress that the sensitivity of the observables on r_{cut} changes if we choose another reference value; however in practice usually r_{cut} is not one of the parameters tuned during the force field development/optimization.

Non-equilibrium regime LJ fluid

Finally, we have also studied a non-reversible LJ fluid. In more detail, we have checked the effect of an additional non-gradient term in the force in the y -direction i.e. $F^\theta(q) = -\nabla V^\theta(q) - G(q)$, $G(q) = [0, \alpha, 0, 0, \alpha, 0, \dots, 0, \alpha, 0]^T$. $\alpha = 1$ for the irreversible case and the term $G(q)$ is divergence-free. The eigenvalues and dominant eigenvectors are summarized in Table V and the corresponding RDF plot is given for comparison in Figure 7. We expected that despite the fact that this process has a different measure close to the stationary measure of the reversible one, the extra non-gradient term cancels out in eq. (6). Hence our results as expected are similar but we have demonstrated that the method is general and can be used for a process equipped with a steady state measure. We aim to the study of more complex systems in non-equilibrium³⁵ in future work.

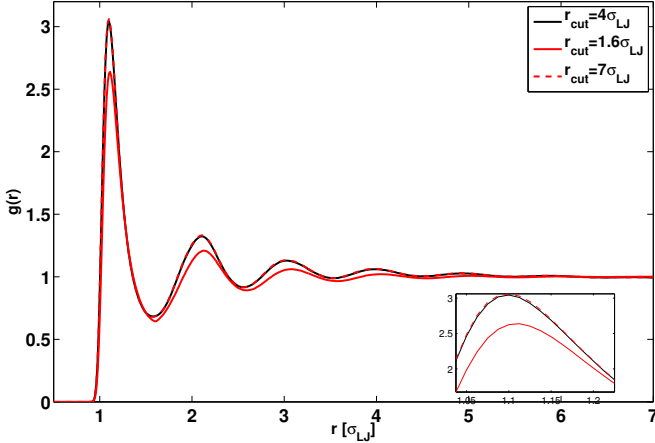


Figure 6. LJ fluid $g(r)$ for different r_{cut} values. Bigger r_{cut} results to longer range attractive forces binding the atoms closer (higher peak). As the L_2 norm quantifies, the influence of almost double r_{cut} value ($4\sigma_{LJ}$ is considered as reference), slightly affects the plot and Pinsker inequality validates this fact. On the other hand, a decrease of this parameter leads to loss of information and the corresponding $g(r)$ describes a completely different model. Note that for this plot we increased the system size as the simulation box dimensions restrict the maximum value of r_{cut} .

$\alpha = 0$		$\alpha = 1$	
eigenvalues	eigenvector	eigenvalues	eigenvector
9.434×10^4	0.062	1.012×10^5	0.0621
4.33×10^{11}	0.998	4.48×10^{11}	0.998

Table V. eigenvalues and eigenvectors for the non-reversible case

B. CH_4

In the following we discuss calculations of RER-FIM as well as various observables for the all-atom methane liquid. FIM and RER calculations are summarized in Figures 8 and 9. In more detail, Figure 8 shows that the RER values vary orders of magnitude for the various parameter perturbations, hence we grouped them in four panels a)-d). In Figure 9 the FIM-based RER data is plotted in logscale for comparison. We note here that due to the uneven number of the different pairs of $C-C$, $C-H$, $H-H$ we have divided with 8 and 16 the quantities corresponding to the second and third type of pairs in order to obtain comparable plots. All RER values are normalized with the number of corresponding interactions. Furthermore, bigger systems consisting of 4000 molecules conclude with identical results.

As in the LJ paradigm, we can see a greater sensitivity on the σ_{LJ} parameters instead of the corresponding ϵ_{LJ} ones. The errorbars indicate that the variance of the estimators were small and that a positive perturbation increased the value of the RER with respect to the

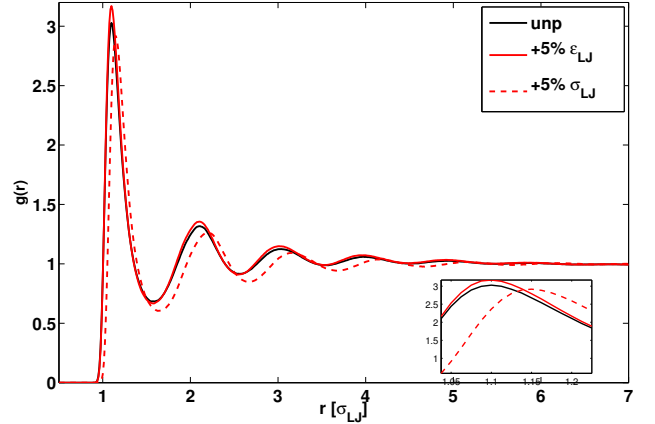


Figure 7. RDF plot for the irreversible case. The norm values are: $\|g^{\theta+5\%\epsilon_{LJ}}(r) - g^{\theta}(r)\|_{L^2} = 0.058$, $\|g^{\theta+5\%\sigma_{LJ}}(r) - g^{\theta}(r)\|_{L^2} = 0.473$

FIM-based RER estimate. Clearly the most sensitive parameter is the $C-H$ bond length r_0 followed by the bending angle θ_0 .

The fact that r_0 and θ_0 are more sensitive is not surprising if we consider that the type of all harmonic potentials is very steep. K_b, K_{θ} constants are of the order $\mathcal{O}(10^2 - 10^{-3})$ as obtained from more detailed (ab initio) calculations or from fittings of experimental data (see Table II). These constants are part of the $\nabla V_{bond}, \nabla V_{angle}$ which is contained in the estimators. The asymmetry in the σ_{LJ} RER values in comparison to the FIM values (panel b in Fig 8) is explained by the third order term contribution in the expansion of RER. A rigorous calculation in Appendix B shows that this term includes the Hessian of the gradient of the potential w.r.t. the parameters and is non-zero for σ_{LJ} .

1. Observables

We perform the same observable computations as with the LJ fluid model in order to validate the predicted sensitivity of the parameters provided by the RER and pathwise FIM methods. Although we have performed simulations for various values of the parameters, we chose 5% as a suitable value for better representation of our results. Note that in principle parameter sensitivities change as we change phase space point; in higher temperatures or low densities each observable is affected differently and our proposed RE method incorporates this behavior through the force differences (eq. 6). Here we have performed simulations in the temperature range from 80 to 180 K and qualitatively similar results were observed. A more detailed study of SA over various temperatures of more complex (macromolecular) systems will be the subject of

perturbation	$\ g^\theta(r) - g^{\theta+\epsilon_0}(r)\ _{L_2}$	$\ g^\theta(r) - g^{\theta-\epsilon_0}(r)\ _{L_2}$
ϵ^{C-C}	1.0×10^{-2}	1.2×10^{-2}
σ^{C-C}	1.1×10^{-1}	5.7×10^{-2}
ϵ^{C-H}	1.7×10^{-2}	9.6×10^{-3}
σ^{C-H}	2.8×10^{-1}	1.7×10^{-1}
ϵ^{H-H}	1.4×10^{-2}	1.15×10^{-2}
σ^{H-H}	2.05×10^{-1}	1.6×10^{-1}
K_b	1.1×10^{-2}	9.7×10^{-3}
r_0	1.01×10^{-1}	1.1×10^{-1}
K_θ	8.7×10^{-3}	8.2×10^{-3}
θ_0	9×10^{-3}	9×10^{-3}

Table VI. L_2 norm of the difference of the unperturbed minus the perturbed $g(r)$ for $\pm 5\%$ perturbation.

a future work.

As in the case of the RDF of the LJ fluid, an increase in the σ_{LJ} parameters shifts the graphs to the right (Figure 10) due to the repulsive forces. All the differences with respect to the L_2 norm are summarized in Table VI for clarity.

In addition, from the set of RDF data presented in Figure 10, an increase in σ_{LJ}^{C-H} values results to larger deviations. As we keep the volume fixed, the contribution of the $C-H$ interactions in the packing is larger than that of the $C-C$ pairs because of the larger number of $C-H$ pairs. Following this graph is the one involving σ_{LJ}^{H-H} increase because of the even smaller numerical value in comparison to the other σ_{LJ} 's. At this point the smaller mass of the hydrogens is the reason although the number of pairs (hence interactions) is the largest.

The MSD plots indicate the $\sigma_{LJ}^{C-H}, \sigma_{LJ}^{H-H}$ as the most sensitive parameters. An increase in σ_{LJ} results to increased collisions and smaller diffusion coefficient (smaller MSD) as can be seen in Figure 11. As in the LJ case, positive σ_{LJ} perturbations (for all three types) result to greater repulsive forces, hence reduced diffusivity. ϵ_{LJ} variations slightly affect the MSD with respect to the other parameters and the same holds for K_b and K_θ too (we have omitted the plots for brevity). Under this dynamic observable the intramolecular interactions are less relevant than the intermolecular ones, for the specific state point (temperature and density) studied here.

Pressure calculations for different perturbation directions are summarized in Table VII. According to this observable quantity σ_{LJ}^{H-H} and r_0 are the most sensitive parameters, which are also indicated by the RE methods. As in the case of the LJ fluid, a change in ϵ_{LJ} (in all pair types) affects the pressure less than a change in σ_{LJ} . Pressure rises through an increase in σ_{LJ} due to more atom collisions. Additionally, stronger forces account for a higher pressure virial. The presented results are in accordance with earlier work⁴³ on an LJ model of water, in which sensitivity analysis using partial derivatives of observables with respect to the parameters were used. That study also demonstrated that pressure is greatly affected

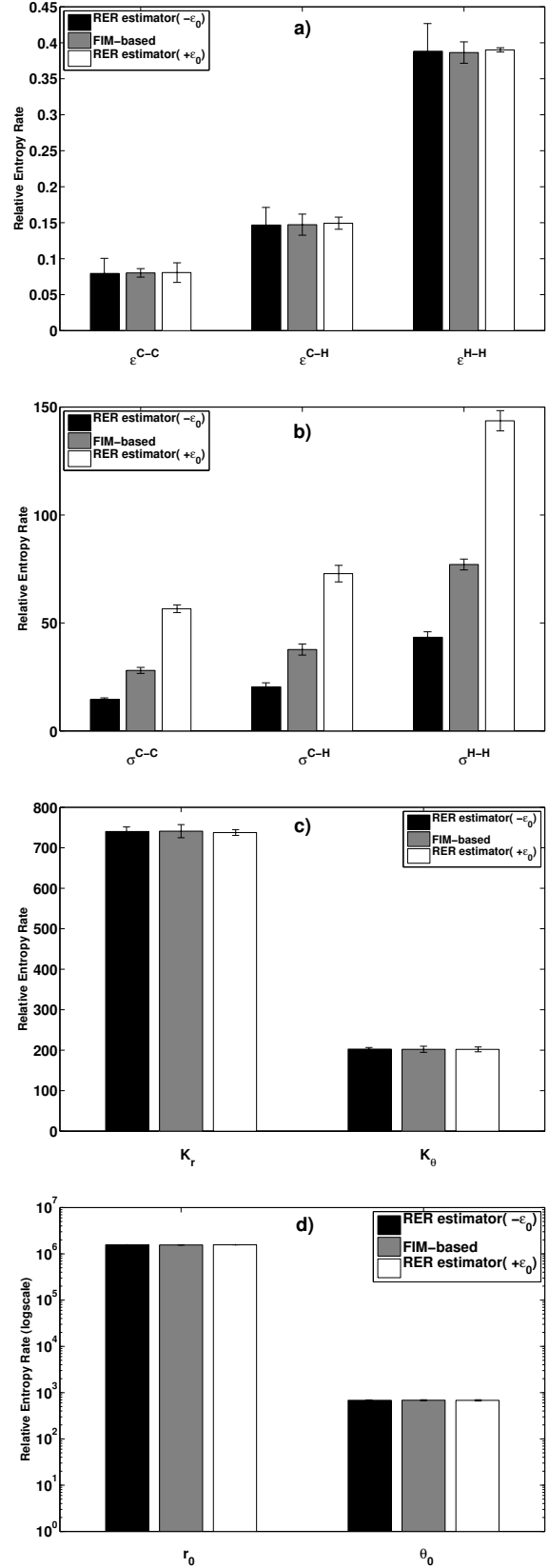


Figure 8. CH_4 per molecule RER-FIM comparison with error bars using the two different estimators for $\pm 5\%$ perturbations in all the parameters. Non-bonded (a and b) and bonded (c and d) potential parameters are shown. The parameters are grouped according to their order of magnitude. The most sensitive one is r_0 followed by θ_0 and there has been a minor scaling according to the number of atom-atom pairs.

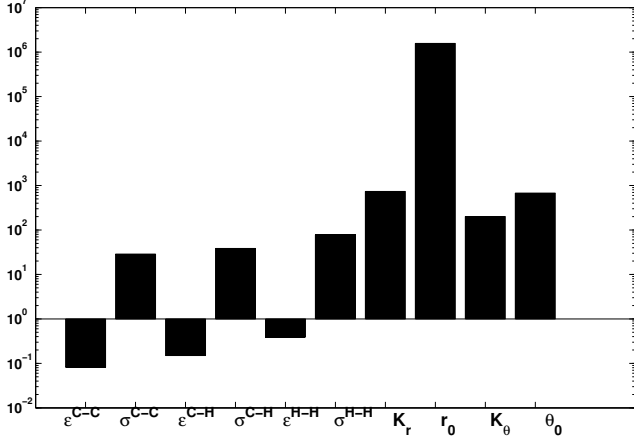


Figure 9. CH_4 FIM-based RER comparison for $\pm 5\%$ perturbations in logscale.

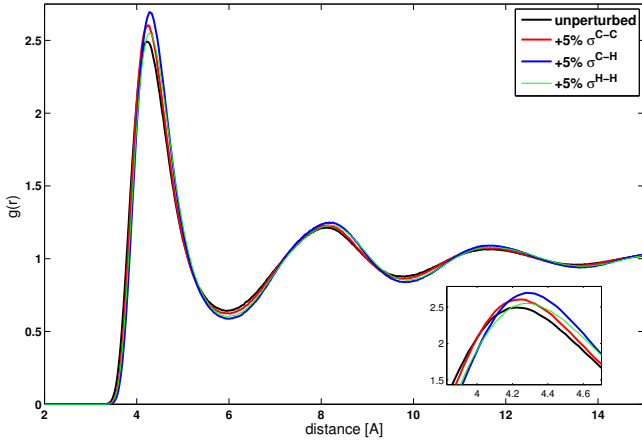


Figure 10. CH_4 molecular $g(r)$ for $+5\%$ perturbations on σ_{LJ} . The tail of the plot varies slightly hence the zoomed region differs more. As in the LJ fluid case, the σ_{LJ} defines the shift of the curve horizontally.

by variations in σ_{LJ} and classified the bond length, σ_{LJ} and the bond constant as the most sensitive ones.

A change in the bending angle θ_0 does not affect the pressure⁴⁴ as well as the impact of the constants K_b, K_θ on the pressure is minimal. We note that the unperturbed system pressure is higher than 1atm because the model we chose (forcefield and integrator) does not reproduce the whole CH_4 phase diagram precisely. Such small deviations from the equations of state and experiments are expected. We refer to the supplementary materials for more figures and results which were omitted here for brevity.

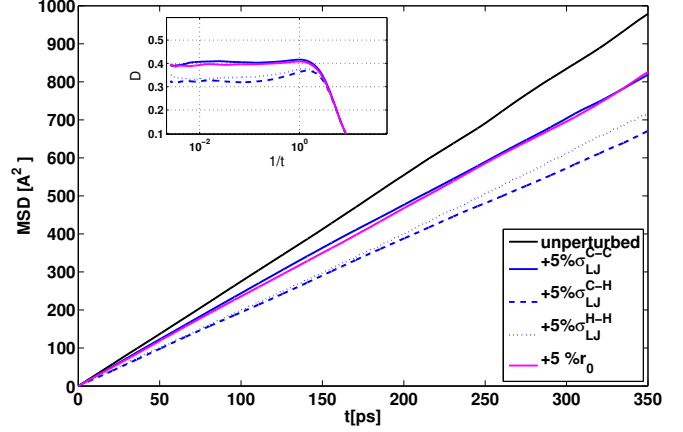


Figure 11. CH_4 MSD for 5% perturbations. We have summarized the most important directions. With respect to this observable, the most sensitive parameter is σ^{C-H} followed by σ^{H-H} . This is in accordance with the RER in Figure 9. The inset illustrates the diffusion coefficient differences in logscale.

perturbation	$P^{\theta+\epsilon_0}$ [atm]	$\frac{P^{\theta+\epsilon_0} - P^\theta}{ P^\theta }$	σ_{STD}	$P^{\theta-\epsilon_0}$ [atm]	$\frac{P^{\theta-\epsilon_0} - P^\theta}{ P^\theta }$
unperturbed	19.7	-	58.4	-	-
ϵ^{C-C}	-3.9	-1.2	51.7	33.1	+0.7
σ^{C-C}	-2.3	-1.1	53.1	87.4	+3.4
ϵ^{C-H}	-31.3	-2.6	52.2	63.6	+2.2
σ^{C-H}	177.2	+8	56.7	44.3	+1.2
ϵ^{H-H}	8.27	-0.6	49.1	23.7	+0.2
σ^{H-H}	437	+21.2	56.3	195	+10.9
K_b	15.3	-0.2	49.6	14.3	-0.3
r_0	281	+13.3	56.5	217	+12
K_θ	18.6	-0.05	52.9	14.9	-0.2
θ_0	13.7	-0.3	52.45	13.3	-0.3

Table VII. Pressure for $\pm 5\%$ perturbation of different directions and the corresponding standard deviation. The most sensitive parameters r_0 and σ^{H-H} increase the pressure substantially.

V. CONCLUSION

In this work, we extended the parametric SA approach of Ref. 12 to stochastic molecular dynamics. The focus was set particularly to the Langevin equation, however, it is applicable to any molecular system that can be described by a system of stochastic differential equations. The presented SA approach is based on the relative entropy per unit time of the path distribution at a reference parameter point with respect to the path distribution at a perturbed parameter point. Major advantages of this method are that: i) it is capable of handling non-equilibrium steady state systems and ii) it is computationally tractable through the expansion of the RER which results in the pathwise FIM. Pathwise FIM provides a fast “gradient-free” method for parametric SA

since it provides an estimate –up to third-order accuracy– of the RER for different perturbation directions through a simple matrix multiplication.

We examined two systems; the well-known prototypical LJ fluid and a more complex one: methane (CH_4). SA on the LJ fluid system was based on the potential parameters $\epsilon_{LJ}, \sigma_{LJ}$ with the latter being the more sensitive to perturbations whereas CH_4 involved 6 intermolecular and 4 intramolecular potential parameters with the intramolecular parameters being the most sensitive in terms of RER. Static and dynamic observable quantities such as the radial distribution function, the mean square displacement and the pressure validated the proposed SA approach. Theoretical justification of the proposed SA approach is also provided through the Pinsker inequality. We also investigated the effect of the potential cutoff radius, r_{cut} , by numerically computing the RER showing first that RER can be used as an information criterion for assigning appropriate values to parameters of the system and second that 5% perturbation of σ_{LJ} produce greater impact than changing r_{cut} from $4\sigma_{LJ}$ to $1.6\sigma_{LJ}$.

Finally, RE for high-dimensional systems was used as a measure of loss of information in coarse-graining.^{13,45,46} Coarse-graining (CG) methods of stochastic systems allow for constructing optimal parametrized Markovian coarse-grained dynamics within a parametric family, by minimizing the information loss (i.e., the relative entropy) on the path space. Application of RE to the error analysis of coarse-graining of stochastic particle systems have been pioneered in these papers.^{47–49} Recent ongoing work on application of the RE framework for CG in the non-equilibrium regime where there’s no Gibbs structure can be found in Ref. 50. We aim to utilize the current SA method to tackle with more complex hybrid macromolecular materials or biomolecular systems in and out-of equilibrium conditions.^{28,29,51} Another goal is to adapt the RE method to quantify and indicate the most efficient CG mapping of mesoscale simulations.⁵²

ACKNOWLEDGMENTS

This research has been co-financed by the European Union (European Social Fund – ESF) and Greek national funds through the Operational Program “Education and Lifelong Learning” of the National Strategic Reference Framework (NSRF) – Research Funding Programs: THALES and ARISTEIA II. The research of MAK was supported in part by the Office of Advanced Scientific Computing Research, U.S. Department of Energy under Contract No. DE-FG02-13ER26161/DE-SC0010723.

Appendix A: Pathwise SA at the discrete-time level

In Section II, we perform SA by first deriving RER and the corresponding pathwise FIM for the continuous-time stochastic Langevin process and then discretizing the process to get numerical estimates for these quantities. We can reverse the order of SA and first discretize the Langevin process and then derive the RER and the pathwise FIM. Here, the latter approach is presented using the BBK algorithm as a numerical integrator of the Langevin process which defines a discrete-time Markov chain. A preliminary example of this approach can be found in Ref. 12. In the BBK integrator, the Hamiltonian part of the Langevin equation (1) is integrated with the Verlet propagator whereas the thermostat is an Ornstein-Uhlenbeck process and the explicit/implicit propagator is used.

The BBK algorithm³² reads

$$\begin{cases} p_{i+\frac{1}{2}} = p_i - \nabla V(q_i) \frac{\Delta t}{2} - \gamma M^{-1} p_i \frac{\Delta t}{2} + \sigma \Delta W_i \\ q_{i+1} = q_i + \Delta t M^{-1} p_{i+\frac{1}{2}} \\ p_{i+1} = p_{i+\frac{1}{2}} - \nabla V(q_{i+1}) \frac{\Delta t}{2} - \gamma M^{-1} p_{i+1} \frac{\Delta t}{2} + \sigma \Delta W_{i+\frac{1}{2}} \end{cases} \quad (\text{A1})$$

$\Delta W_i, \Delta W_{i+\frac{1}{2}}$ are iid Gaussian random vectors with zero mean and covariance matrix $\frac{\Delta t}{2} I_{dN}$ while Δt is the time step of the numerical scheme. Notice that other choices of numerical integrators can be utilized such as the ones proposed by Leimkuhler et al.^{36,53} which introduce a relatively weak perturbative effect on the physical dynamics.

We define the state of the discrete-time system at time-step i as $z_i = (q_i, p_i) \in \mathbb{R}^{2dN}$. The process $\{z_i\}_{i=0}^M$ for the BBK integrator is a Markov chain with transition probability $P^\theta(z_i, z_{i+1})$ where $\theta \in \mathbb{R}^K$ is the vector of the system’s parameters. Notice that the length of the discrete-time process is related with the time window of the continuous-time process through $T = M\Delta t$. The path space probability density, $\bar{Q}_{0:M}^\theta(\cdot)$, is defined as

$$\bar{Q}_{0:M}^\theta(\{z_i\}_{i=0}^M) = \bar{\mu}^\theta(z^0) \prod_{i=0}^{M-1} P^\theta(z_i, z_{i+1}), \quad (\text{A2})$$

where $\bar{\mu}^\theta(\cdot)$ denotes the stationary distribution of the discrete-time. As in the continuous-time case, we perturb the parameter vector, θ , by adding a perturbation vector $\epsilon_0 \in \mathbb{R}^K$. At the stationary regime, the pathwise relative entropy of $\bar{Q}_{0:M}^\theta$ with respect to $\bar{Q}_{0:M}^{\theta+\epsilon_0}$ admits also a decomposition into a linear in time term plus a constant.¹² Indeed, it holds that

$$\mathcal{R}(\bar{Q}_{0:M}^\theta | \bar{Q}_{0:M}^{\theta+\epsilon_0}) = M\mathcal{H}(\bar{Q}^\theta | \bar{Q}^{\theta+\epsilon_0}) + \mathcal{R}(\bar{\mu}^\theta | \bar{\mu}^{\theta+\epsilon_0}), \quad (\text{A3})$$

where $\mathcal{R}(\bar{\mu}^\theta | \bar{\mu}^{\theta+\epsilon_0})$ is the relative entropy between the stationary distributions while $\mathcal{H}(\bar{Q}^\theta | \bar{Q}^{\theta+\epsilon_0})$ is the RER of the discrete-time Markov chain given by

$$\mathcal{H}(\bar{Q}^\theta | \bar{Q}^{\theta+\epsilon_0}) = \mathbb{E}_{\bar{\mu}^\theta} \left[\int_{\mathbb{R}^{2dN}} P^\theta(z, z') \log \frac{P^\theta(z, z')}{P^{\theta+\epsilon_0}(z, z')} dz' \right]. \quad (\text{A4})$$

The discrete-time RER is related with the continuous-time RER through⁵²

$$\mathcal{H}(Q^\theta|Q^{\theta+\epsilon_0}) = \lim_{\Delta t \rightarrow 0} \frac{1}{\Delta t} \mathcal{H}(\bar{Q}^\theta|\bar{Q}^{\theta+\epsilon_0}). \quad (\text{A5})$$

As expected, discrete-time RER is locally a quadratic functional in a neighborhood of θ hence its curvature around θ , defined by the Hessian, is the pathwise FIM which is given by¹²

$$F_{\mathcal{H}}(\bar{Q}^\theta) = \mathbb{E}_{\mu^\theta} \left[\int_{\mathbb{R}^{2dN}} P^\theta(z, z') \nabla_\theta \log P^\theta(z, z') \nabla_\theta \log P^\theta(z, z')^T dz' \right]. \quad (\text{A6})$$

We refer to (12) for statistical estimators of the discrete-time RER and the corresponding pathwise FIM while in Supplementary Materials we provide detailed formulas for the numerical calculation of (A4) and (A6) for the BBK integrator.

Appendix B: Expansion of the continuous-time RER

We now expand the RER in eq. (6) through Taylor series expansion around the point θ . We start with expanding the m -th component of the force, $F_m^{\theta+\epsilon_0}(q)$, around θ

$$F_m^{\theta+\epsilon_0}(q) = F_m^\theta(q) + \nabla_\theta F_m^\theta(q) \epsilon_0 + \frac{1}{2} \epsilon_0^T \nabla_\theta^2 F_m^\theta(q) \epsilon_0 + \mathcal{O}(|\epsilon_0|^3) \quad (\text{B1})$$

where ∇ denotes the $1 \times K$ gradient vector while ∇^2 denotes the $K \times K$ Hessian matrix. Then, the RER is written as

$$\begin{aligned} \mathcal{H}(Q^\theta|Q^{\theta+\epsilon_0}) &= \frac{1}{2} \mathbb{E}_{\mu^\theta} [(F_m^{\theta+\epsilon_0}(q) - F_m^\theta(q))^T (\sigma \sigma^T)^{-1} (F_m^{\theta+\epsilon_0}(q) - F_m^\theta(q))] \\ &= \frac{1}{2} \sum_{m,n=1}^{dN} \mathbb{E}_{\mu^\theta} [(F_m^{\theta+\epsilon_0}(q) - F_m^\theta(q)) ((\sigma \sigma^T)^{-1})_{m,n} (F_n^{\theta+\epsilon_0}(q) - F_n^\theta(q))] \quad \text{where} \\ &= \frac{1}{2} \sum_{m,n=1}^{dN} ((\sigma \sigma^T)^{-1})_{m,n} \mathbb{E}_{\mu^\theta} [\nabla_\theta F_m^\theta(q) \epsilon_0 \nabla_\theta F_n^\theta(q) \epsilon_0] \\ &+ \frac{1}{2} \sum_{m,n=1}^{dN} ((\sigma \sigma^T)^{-1})_{m,n} \mathbb{E}_{\mu^\theta} [\nabla_\theta F_m^\theta(q) \epsilon_0 \epsilon_0^T \nabla_\theta^2 F_n^\theta(q) \epsilon_0] + \mathcal{O}(|\epsilon_0|^4). \end{aligned}$$

The pathwise FIM comes from the second-order term while the third-order term defines a tensor matrix.

For the LJ non-bonded potential, the leading term of the second-order term (i.e., the pathwise FIM) in the RER expansion when σ_{LJ} is perturbed is of order $O\left(\left(\frac{\sigma_{LJ}}{r}\right)^{10}\right)$ while the leading term of the third-order term of RER is of order $O\left(\left(\frac{\sigma_{LJ}}{r}\right)^9\right)$ with (typically) $\sigma_{LJ} < r$. The fact that the leading term of the third-order term has smaller exponent compared to the second-order term, makes the contribution of the

third-order term to the value of RER significant on average. Therefore, the asymmetry between $\mathcal{H}(Q^\theta|Q^{\theta+\epsilon_0})$ and $\mathcal{H}(Q^\theta|Q^{\theta-\epsilon_0})$ observed both in the LJ fluid (Figure 2) and the methane (Figure 8) stems exactly from the significance of the third-order term. Notice that asymmetries between positive and negative perturbations are not rare and have been observed in biological reaction models and one method that is employed for assessing parameter identifiability in non-linear models is the profile likelihood method.⁵⁴

Appendix C: Potential energy terms of CH_4

In this section, the details of the total potential $V(q) = V_{bond}(q) + V_{angle}(q) + V_{LJ}(q)$ for the methane model are presented. The total bond potential equals to

$$V_{bond}(q) = \sum_{\mathcal{A}} V_{bond}(|q_j - q_i|) \quad (\text{C1})$$

where

$$\mathcal{A} = \{q_i=C, q_j=H \mid q_i, q_j \in \text{same } CH_4, \text{ 4 bonds per } CH_4\}$$

while the local bond potential is

$$V_{bond}(|q_j - q_i|) = V_{bond}(r_{ij}) = \frac{1}{2} K_b (r_0 - q_{ij})^2. \quad (\text{C2})$$

The two constants r_0 and K_b determine the distance and the strength of the bond between the two atoms, respectively.

The angle defined for each triplet $H-C-H$ on the same CH_4 molecule is denoted by θ_{ijk} . Then, the total angular potential is

$$V_{angle}(q) = \sum_{\mathcal{B}} V_{angle}(\angle q_j q_i q_k) \quad (\text{C3})$$

$$\mathcal{B} = \{q_i=C, q_j, q_k=H, q_i, q_j, q_k \in \text{same } CH_4, \text{ 6 angles per } CH_4\},$$

while the local angular potential is given by

$$V_{angle}(\angle q_j q_i q_k) = V_{angle}(\theta_{ijk}) = \frac{1}{2} K_\theta (\theta_0 - \theta_{ijk})^2. \quad (\text{C4})$$

The two constants θ_0 and K_θ determine the degree and the strength of the angle, respectively.

Moreover, the non-bonded term of the potential energy, $V_{LJ}(q)$, is given by

$$V_{LJ}(q) = \sum_{\mathcal{C}} V_{LJ}(|q_j - q_i|) \quad (\text{C5})$$

where

$$\mathcal{C} = \{q_i, q_j=H \text{ or } C, q_i, q_j \in \text{different } CH_4\}$$

while the functional form of the LJ potential, $V_{LJ}(r_{ij})$, is given by (17).

Since the LJ potential is the non-bonded term, the sum in (C5) is over all the atoms of the other methanes. It is convenient furthermore to divide this sum into three sums, each one corresponding on a different class of interactions between $C - C, C - H, H - H$. Thus, we can rewrite

$$V_{LJ}(q) = \sum_{c_1} V_{LJ}^{C-C}(r_{ij}) + \sum_{c_2} V_{LJ}^{H-H}(r_{ij}) + \sum_{c_3} V_{LJ}^{H-C}(r_{ij}), \quad (\text{C6})$$

where

$$\begin{aligned} C_1 &= \{q_i, q_j = C\} \\ C_2 &= \{q_i = C, q_j = H, q_i, q_j \in \text{different } CH_4\} \\ C_3 &= \{q_i, q_j = H, q_i, q_j \in \text{different } CH_4\}. \end{aligned}$$

Each LJ potential has its own parameter values.

REFERENCES

- ¹M. P. Allen and D. J. Tildesley. *Computer simulation of liquids*. Clarendon Press, New York, NY, USA, 1987.
- Daan Frenkel and B. Smit. *Understanding Molecular Simulation, Second Edition: From Algorithms to Applications (Computational Science)*. Academic Press, 2001.
- ²M.J. Kotelyanskii and D.N. Theodorou. *Simulation Methods for Polymers*, volume Chapter "Molecular Dynamics Simulations of Polymers". Marcel Dekker, New York, 2004.
- ³D. E. Shaw, P. Maragakis, K. Lindorff-Larsen, S. Piana, R. Dror, M. P. Eastwood, J. A. Bank, J. M. Jumper, J Salmon, Y. Shan, and W. Wriggers. Atomic-level characterization of the structural dynamics of proteins. *Science*, 330(6002):341–346, 2010.
- ⁴D. Fritz, V. A. Harmandaris, K. Kremer, and N. Van der Vegt. Coarse-grained polymer melts based on isolated atomistic chains: simulation of polystyrene of different tacticities. *Macromolecules*, 42(19):7579–7588, 2009.
- ⁵V. Johnston and V. Harmandaris. Hierarchical simulations of hybrid polymer/solid materials. *Soft Matter*, 9:6696–6710, 2013.
- ⁶A. Chernatynskiy, S. Phillpot, and R. LeSar. Uncertainty quantification in multiscale simulation of materials: A prospective. *Annual review of Materials Research*, 43:157–182, July 2013.
- ⁷P. Angelikopoulos, C. Papadimitriou, and P. Koumoutsakos. Bayesian uncertainty quantification and propagation in molecular dynamics simulations: A high performance computing framework. *J. Chem. Phys.*, 137(14), 2012.
- ⁸H. Liu, A. Sudjianto, and W. Chen. Relative entropy based method for probabilistic sensitivity analysis in engineering design. *Journal of Mechanical Design*, 128(2):326–336, 2005.
- ⁹F. Cailliez and P. Pernot. Statistical approaches to forcefield calibration and prediction uncertainty in molecular simulation. *J Chem. Phys.*, 134(5), 2011.
- ¹⁰F. Rizzi, H. N. Najm, B. J. Debuschere, K. Sargsyan, M. Salloum, H. Adalsteinsson, and O. M. Knio. Uncertainty quantification in md simulations. part i: forward propagation. *SIAM Multiscale Model. Simul.*, 10(4):1428–1459, 12 2012.
- ¹¹S. K. Rao, R. Imam, K. Ramanathan, and S. Pushpavanam. Sensitivity analysis and kinetic parameter estimation in a three way catalytic converter. *Industrial & Engineering Chemistry Research*, 48:3779–3790, 2009.
- ¹²Y. Pantazis and M. Katsoulakis. A relative entropy rate method for path space sensitivity analysis of stationary complex stochastic dynamics. *J. Chem. Phys.*, 138, 2013.
- ¹³A. F. Emery and A. V. Nenarokomov. Optimal experiment design. *Measurement Science and Technology*, 9(6):864, 1998.
- ¹⁴B. Cooke and S. C. Schmidler. Statistical prediction and molecular dynamics simulation. *Biophysical Journal*, 95:4497–4511, November 2008.
- ¹⁵R. D. Braatz, R. C. Alkire, E. Seebauer, E. Rusli, R. Gunawan, T.O. Drews, X. Li, and Y. He. Perspectives on the design and control of multiscale systems. *J. Proc. Control*, 16:193–204, 2006.
- ¹⁶R. Gunawan, Y. Cao, L. Petzold, and F. J. III Doyle. Sensitivity analysis of discrete stochastic systems. *Biophysical Journal*, 88:2530–2540, 2005.
- ¹⁷M. Rathinam, P. W. Sheppard, and M. Khammash. Efficient computation of parameter sensitivities of discrete stochastic chemical reaction networks. *J. Chem. Phys.*, 132:034103–(1–13), 2010.
- ¹⁸D. F. Anderson. An efficient finite difference method for parameter sensitivities of continuous-time Markov chains. *SIAM J. Numerical Analysis*, 50(5):2237–2258, 2012.
- ¹⁹G. Arampatzis and M. A. Katsoulakis. Goal-oriented sensitivity analysis for lattice kinetic monte carlo simulations. *J. Chem. Phys.*, 12(140):124108, 2014.
- ²⁰P. W. Glynn. Likelihood ratio gradient estimation for stochastic systems. *Communications of the ACM*, 33(10):75–84, 1990.
- ²¹S. Plyasunov and A. P. Arkin. Efficient stochastic sensitivity analysis of discrete event systems. *J. Comput. Phys.*, 221(2):724–738, February 2007.
- ²²P. B. Warren and R. J. Allen. Steady-state parameter sensitivity in stochastic modeling via trajectory reweighting. *J. Chem. Phys.*, 136(10), 2012.
- ²³T. Iordanov, G. Schenter, and B. Garret. Sensitivity analysis of thermodynamic properties of liquid water: a general approach to improve empirical potentials. *J. Phys. Chem*, A(110):762–771, 2006.
- ²⁴A. Majda and B. Gershgorin. Quantifying uncertainty in climate change science through empirical information theory. *PNAS*, 107(34):14958–14963, 2010.
- ²⁵C. Baig and V. Harmandaris. Quantitative analysis

- on the validity of a coarse-grained model for nonequilibrium polymeric liquids under flow. *Macromolecules*, (43):3156–3160, 2010.
- ²⁶K. R. Haas, H. Yang, and J-W Chu. Fisher information metric for the Langevin equation and least informative models of continuous stochastic dynamics. *J. Chem. Phys.*, 139(12), SEP 28 2013.
- ²⁷V. Johnston and V. Harmandaris. Hierarchical multi-scale modeling of polymer–solid interfaces: Atomistic to coarse-grained description and structural and conformational properties of polystyrene–gold systems. *Macromolecules*, 46:5741–5750, 2013.
- ²⁸A. Rissanou and V. Harmandaris. Dynamics of various polymer/graphene interfacial systems through atomistic molecular dynamics simulations. *Soft Matter*, 42(10):2876–2888, 2014.
- ²⁹V. Harmandaris. Quantitative study of equilibrium and non-equilibrium polymer dynamics through systematic hierarchical coarse-graining simulations. *Korea-Aust. Rheol. J.*, 26:15–28, 2014.
- ³⁰B. Smit. Phase diagrams of lennard-jones fluids. *J. Chem. Phys*, 96(11), 6 1992.
- ³¹S. Mayo, B. Olafson, and W. Goddard. Dreiding: a generic force field for molecular simulations. *J. Phys. Chem.*, 94(26):8897–8909, 1990.
- ³²T. Lelievre, M. Rousset, and G. Stoltz. *Free energy calculations*. Imperial College Press, 2010.
- ³³T Cover and J. Thomas. *Elements of Information Theory*. John Wiley and Sons, 1991.
- ³⁴B. Oksendal. *Stochastic Differential Equations: An introduction with applications*. Springer-Verlag, 5th edition, 2000.
- ³⁵V. Harmandaris, V. Mavrantzas, and D. Theodorou. Atomistic molecular dynamics simulation of stress relaxation upon cessation of steady-state uniaxial elongational flow. *Macromolecules*, 33(21):8062–8076, 2000.
- ³⁶B. Leimkuhler and C. Matthews. Robust and efficient configurational molecular sampling via langevin dynamics. *J. Chem. Phys*, 138(17), 2013.
- ³⁷V. Bally and D. Talay. The law of the Euler scheme for stochastic differential equations. I. Convergence rate of the distribution function. *Probab. Theory Related Fields*, 104:43–60, 1996.
- ³⁸V. Bally and D. Talay. The law of the Euler scheme for stochastic differential equations. II. Convergence rate of the density. *Monte Carlo Methods Appl.*, 2:93–128, 1996.
- ³⁹J. C. Mattingly, A. M. Stuart, and M. V. Tretyakov. Convergence of numerical time-averaging and stationary measures via Poisson equations. *SIAM J. Numer. Anal.*, 48:552–577, 2010.
- ⁴⁰P. Dupuis, M.A. Katsoulakis, Y. Pantazis, and P. Plecháč. Sensitivity bounds and error estimates for stochastic models. (*in preparation*).
- ⁴¹D. A. Hensher and K. J. Button. *Handbook of Transport and the Environment*. Elsevier, 2003.
- ⁴²D. McQuarrie. *Statistical Mechanics*. Harper Collins Publishers, 1976.
- ⁴³S. B. Zhu and C. F. Wong. Sensitivity analysis of a polarizable water model. *J. Chem. Phys*, 98:4695–4701, 1994.
- ⁴⁴H. Heinz, W. Paul, and K. Binder. Calculation of local pressure tensors in systems with many-body interactions. *Phys. Rev. E*, 72(6):066704–066714, 2005.
- ⁴⁵M. S. Shell. Systematic coarse-graining of potential energy landscapes and dynamics in liquids. *J. Chem. Phys*, 137(8), 2012.
- ⁴⁶M. A. Katsoulakis, P. Plecháč, L. Rey-Bellet, and D. K. Tsagkarogiannis. Coarse-graining schemes and a posteriori error estimates for stochastic lattice systems. *ESAIM: Mathematical Modelling and Numerical Analysis*, 41:627–660, 5 2007.
- ⁴⁷M. A. Katsoulakis, A. J. Majda, and D. G. Vlachos. Coarse-grained stochastic processes for microscopic lattice systems. *Proc. Natl. Acad. Sci. USA*, 100(3):782–787, 2003.
- ⁴⁸M. A. Katsoulakis, A. J. Majda, and D. G. Vlachos. Coarse-grained stochastic processes and monte carlo simulations in lattice systems. *J. Comp. Phys.*, 112:250–278, 2003.
- ⁴⁹M. A. Katsoulakis, L. Rey-Bellet, P. Plecháč, and D. K. Tsagkarogiannis. Mathematical strategies in the coarse-graining of extensive systems: error quantification and adaptivity. *J. Non Newt. Fluid Mech.*, 2008.
- ⁵⁰M. A. Katsoulakis and P. Plecháč. Information-theoretic tools for parametrized coarse-graining of non-equilibrium extended systems. *J. Chem. Phys.*, 139(arXiv:1304.7700), Apr 2013.
- ⁵¹A. Rissanou, E. Georgilis, M. Kasotakis, A. Mitraki, and V. Harmandaris. Effect of solvent on the self-assembly of dialanine and diphenylalanine peptides. *J. Phys. Chem. B*, 117:3962–3975, 2013.
- ⁵²E. Kalligiannaki, V. Harmandaris, M. Katsoulakis, and P. Plecháč. Optimizing coarse-grained models for non-equilibrium molecular systems: Dynamical force matching across scales. *to be submitted*.
- ⁵³B. Leimkuhler, E. Noorizadeh, and F. Theil. A gentle stochastic thermostat for molecular dynamics. *J. Stat. Phys.*, (135):261–277, 2009.
- ⁵⁴A. Raue, C. Kreutz, T. Maiwald, J. Bachmann, M. Schilling, U. Klingmüller, and J. Timmer. Structural and practical identifiability analysis of partially observed dynamical models by exploiting the profile likelihood. *Bioinformatics*, 2009.